Exploring the Contribution of Collective Motions to the Dynamics of Forced-Unfolding in Tubulin

Harshad Joshi,[†] Farhana Momin,[‡] Kelly E. Haines,[†] and Ruxandra I. Dima[†*]
[†]Department of Chemistry, University of Cincinnati, Cincinnati, Ohio; and [‡]Department of Chemistry, Mount Holyoke College, Holyoke, Massachusetts

ABSTRACT Decomposition of the intrinsic dynamics of proteins into collective motions among distant regions of the protein structure provides a physically appealing approach that couples the dynamics of the system with its functional role. The cellular functions of microtubules (an essential component of the cytoskeleton in all eukaryotic cells) depend on their dynamic instability, which is altered by various factors among which applied forces are central. To shed light on the coupling between forces and the dynamic instability of microtubules, we focus on the investigation of the response of the microtubule subunits (tubulin) to applied forces. We address this point by adapting an approach designed to survey correlations for the equilibrium dynamics of proteins to the case of correlations for proteins forced-dynamics. The resulting collective motions in tubulin have a number of functional implications, such as the identification of long-range couplings with a role in blocking the dynamic instability of microtubules. A fundamental implication of our study for the life of a cell is that, to increase the likelihood of unraveling of large cytoskeletal filaments under physiological forces, molecular motors must use a combination of pulling and torsion rather than just pulling.

INTRODUCTION

Correlations between motions of positions that are far away in the sequence and/or in the three-dimensional structural fold of a protein are increasingly recognized as crucial functional elements of proteins. This is especially true for positions involved in allosteric communications (1–3) and, as recently highlighted, in enzymatic activity (4–6). The details of allosteric transitions can be gleaned from the analysis of the equilibrium collective motions in the protein. Thus, the highly dynamic changes driven by the force-induced unfolding or indentation of large polymeric structures such as cytoskeletal filaments (7–9) and viral capsids (10) are perfect candidates for a description based on the division of a protein fold into dynamical domains (6,11). The nonequilibrium character of these large-scale transformations makes the identification of dynamical domains particularly challenging because they are likely to evolve with time as the fold of the protein is altered by unfolding/indentation. For example, unfolding of one region of the protein can induce the formation of new dynamical domains in different, still folded, regions of the protein depending on their ability to align on the direction of pulling.

MTs are composed of protofilaments aligned in parallel and joined laterally (12) consisting of α- and β-tubulin dimers (8 nm in length) connected noncovalently along the longitudinal axis of the filament. During interphase, the (–) end (α-tub) is attached to the centrosome, whereas the (+) end (β-tub) has a GTP cap containing at least one layer of GTP β-tub (13,14). Conversely, during mitosis, the (–) end breaks from the centrosome and MTs depolymerize and polymerize fast, i.e., undergo dynamic instability—stochastic alternation of slow growth and rapid shrinking phases between MTs and soluble tubulin subunits (7). The monomers, α-tub (440 residues) and β-tub (427 residues), have very similar structures consisting of a *N*-terminal nucleotide (GTP or GDP) binding domain, an intermediate taxol binding domain (in β-tub), and a C-terminal microtubule-associated protein binding domain comprising residues 1–205, 206–381, and 382–440, respectively (15). The mechanical properties of MTs play a crucial role in cell division and matrix remodeling induced by mechanical loading (16–19). Understanding the microscopic principles governing MT instability (7,13) and breaking of the (–) end from the centrosome, which are relevant also for axonal guidance in new directions (20), is therefore vital for understanding basic cellular processes. In cells, protein factors such as katanin and spastin induce severing of MTs by force (21).

To shed light on these processes:

1. One needs to capture the range of forces that induce their breaking.
2. One needs to uncover the submolecular details of the associated structural changes.

The first issue was addressed in our previous studies of force-induced unfolding of the tubulin heterodimer and its monomers under force-ramp conditions that are experimentally relevant (22). By employing molecular simulations of a self-organized polymer (SOP) model of the tubulin units (23), our extensive simulations revealed that, in isolation, each monomer unfolds according to two pathways leading to different force-extension curves (FECs). However, the tubulin dimer unfolds according to a unique pathway irrespective of the scenario of application of force (22). In this study, we address the second issue through the analysis of the collective motions that induce each breaking event in

Submitted July 15, 2009, and accepted for publication October 27, 2009.

*Correspondence: ruxandra.dima@uc.edu or dimari@ucmail.uc.edu

Editor: Nathan Andrew Baker.

0006-3495/10/02/0657/10 $2.00

doi: 10.1016/j.bpj.2009.10.043

the FECs of tubulin dimer and of its subunits. This is equivalent to the identification of dynamical domains during the nonequilibrium unfolding of large proteins.

A variety of methods have been developed to identify dynamical domains in a protein at equilibrium or to generate pathways between two distinct equilibrium states of a protein (6,11,24–26). Most of these methods rely on a single conformation of the protein by starting from the information provided by normal mode analysis or by essential dynamics such as on cross correlations between positions. These approaches have been tested with very good success, so the development of yet another such method is not our goal. Instead, in light of the nonequilibrium character of the forced-unfolding process in proteins, the focus of our investigation is to determine, from the forced-unfolding data, physically relevant covariations that can be subsequently used as a starting point in methods such as the ones above. Consequently, after calculating the input data, we employ a methodology reminiscent of Yesylevskyy et al. (26) and Keskin et al. (27) to extract the dynamical domains.

Although the interpretation of averages for systems in nonequilibrium is challenging, for a system starting far-from equilibrium in a concave potential that will eventually reach equilibrium, time-averaged correlations do not depend on the starting state. Therefore, nonequilibrium and equilibrium correlations coincide (28–30). In dynamic force spectroscopy, unbinding experiments systems start in far-from equilibrium states and the rate of rupture of bonds under force is determined based on Kramer's theory (31–34). The theoretical treatment of the forced-unfolding of proteins must account for their intrinsic rugged energy landscape (31,35). As a result, the mechanical unfolding of a protein can be modeled as an escape over a cascade of many sharp barriers. Determination of the unfolding rate under these conditions employs Kramer's' stationary flux method (31) that assumes near-equilibration of states over regions of the energy landscape below the principal barriers. In other words, upon completion of an unfolding event as signaled by a sudden increase (decrease) in the extension (force), the protein reaches quasiequilibrium in the new basin of attraction (local potential energy minimum) and retains this state until the escape over the next tall barrier. In summary, the unfolding process is quasiadiabatic, which holds well when the applied force does not increase fast (i.e., increases at rates used in experiments) (34). A consequence of quasiadiabaticity is that the bound system is in near-equilibrium even in the presence of force, i.e., the timescale for equilibration is much shorter than the time for the calculation of correlations.

We extract the matrix of interresidue three-dimensional orientational correlations obtained before each of the main transition points during the unfolding, i.e., before each peak in the FEC. This takes advantage of the near-equilibrium state of the system in each individual basin of attraction. Because ergodicity is also important, we build the correlations as a double average: over the conformations from a basin and over the trajectories presenting this basin. Analysis of patterns of similarity in these matrices, either directly or by employing a clustering method (36), yields the main dynamic clusters of positions similar to approaches used for equilibrium correlations (26,27). Because of the highly constrained dynamics of a protein during forced-unfolding, we next decomposed the motion of the chain into its components on the direction of pulling and in the plane perpendicular to this direction, and we extracted the corresponding correlations. This enables us to dissect the contribution of rotational versus translational motion to the unfolding pathway. The final part of our analysis pertains to directly following the propagation of tension in the chain, while accounting for any possible refolding of the previously unraveled chain segments. This allows us, for example, to determine whether the force-regime employed in our simulations biases the unfolding pathway(s) (23). The information yielded by our three-layered approach provides a detailed picture of the contribution of dynamical domains to the unfolding process, and this correlates with functional aspects of tubulin and MTs as noted below.

METHODS

SOP-model simulations

To conduct mechanical unfolding studies of tubulin and its subunits, we used a model based on the topology of the chain in which each amino acid in the Protein Data Bank (PDB) (36) entry 1tub is represented by its C_α atom (23). The total energy function for a conformation, specified in terms of the coordinates $\{r_i\}$ ($i = 1, 2, \cdots N$), where N is the number of residues is

$$\begin{aligned} V_T &= V_{FENE} + V_{NB}^{ATT} + V_{NB}^{REP} \\ &= -\sum_{i=1}^{N-1} \frac{k}{2} R_0^2 \log\left(1 - \frac{\left(r_{i,i+1} - r_{i,i+1}^0\right)^2}{R_0^2}\right) \\ &\quad + \sum_{i=1}^{N-3} \sum_{j=i+3}^{N} \varepsilon_h \left[\left(\frac{r_{ij}^o}{r_{ij}}\right)^{12} - 2\left(\frac{r_{ij}^o}{r_{ij}}\right)^6\right] \Delta_{ij} \\ &\quad + \sum_{i=1}^{N-2} \varepsilon_l \left(\frac{\sigma_{i,i+2}}{r_{i,i+2}}\right)^6 + \sum_{i=1}^{N-3} \sum_{j=i+3}^{N} \varepsilon_l \left(\frac{\sigma}{r_{ij}}\right)^6 (1 - \Delta_{ij}). \end{aligned} \tag{1}$$

The distance between two neighboring interaction sites i and $i + 1$ is $r_{i,\,i+1}$, whereas $r_{i,i+1}^o$ is its value in the native structure. The first term in Eq. 1 describes the backbone chain connectivity. The second term accounts for the interactions that stabilize the native state. If the noncovalently linked beads i and j for $|i - j| > 2$ are within a cutoff distance R_C (i.e., $r_{ij} < R_C$) then $\Delta_{ij} = 1$. If $r_{ij} > R_C$, then $\Delta_{ij} = 0$. A uniform value for ε_h, which specifies the strength of the nonbonded interactions, is assumed. All nonnative interactions (third and fourth terms in Eq. 1) are repulsive.

The unfolding of the molecule was followed by performing Brownian dynamics simulations at $T = 300$ K. Following the typical AFM experimental setup (38), the C-terminal end of each monomer was stretched at two constant pulling speeds typically employed for such experiments ($v = 1.9$ μm/s and $v = 19$ μm/s) while keeping the N-terminal end fixed. For the dimer simulations, we used three different pulling setups as described in Dima and Joshi (22). (Values of the parameters used in the simulations are given in (22).) In all cases, the force was applied along

the x axis. Because previously the results did not depend dramatically on the exact value of the speed, here we analyzed only the trajectories obtained at the higher value of v.

Correlation analysis

The pairwise correlations, measuring the standard interresidue three-dimensional orientational coupling, are computed, following Chen et al. (4), using the time-averaged covariance matrix as

$$\langle C_{ij} \rangle = \sum_{n=1}^{M} \frac{1}{T_{obs}} \int_0^{T_{obs}} \Delta \widehat{\mathbf{r}_i^{(n)}}(t) \cdot \Delta \widehat{\mathbf{r}_j^{(n)}}(t) dt, \qquad (2)$$

where $\Delta \widehat{\mathbf{r}_i^{(n)}}$ is the unit vector of the displacement of the ith C_α atom at time t, with respect to its initial value along trajectory n, and M is the total number of trajectories that unfold according to a given pathway. T_{obs} is the length of time over which we calculate the covariations which must obey the condition of quasiadiabaticity discussed above. If $\langle C_{ij} \rangle$ is positive, then the motions of the two residues i and j are correlated, whereas negative values correspond to anticorrelation.

Two issues must be addressed before the calculation of $\Delta \widehat{\mathbf{r}_i^{(n)}}$ in Eq. 2:

1. The identification of the appropriate reference structure.
2. The alignment of the current and the reference structures.

For the equilibration phase of the trajectory, the correlations were computed by taking, as reference structure, the native structure of the monomer from the PDB. In addition, we eliminated the contribution of the six degrees of freedom of the molecule, by aligning each structure with the reference structure using the Kabsch algorithm (39).

For the force-induced unfolding phase of the trajectory, the choice for the reference structure is inspired by the setup of the AFM experiments that we model in our simulations:

1. The starting state is selected from the native basin of attraction of the protein.
2. One end of the chain (usually the N-terminus) is kept immobilized on a plate while the other end is being pulled using force-ramp conditions.
3. The stretching of the chain continues until the final rodlike conformation (the minimum free-energy in the presence of force) is reached.

Experimentally, the dynamics of unfolding of the chain is followed with respect to the initial state (highly populated in the absence of force): an unfolding event is signaled by a sudden increase in the chain extension, i.e., the difference between the end-to-end distance of the chain in the current state and the corresponding value in the starting conformation. To enable the comparison with the experiments, we used as reference for the calculation of the spatial correlations the starting (in experiments), at the end of equilibration (in simulations), conformation. This approach is also similar in spirit with the one employed, for example, in Noolandi and Hong (29) to determine the nonequilibrium time-correlations between parts of a highly entangled polymer chain to model real-time, small-angle neutron scattering experiments.

Upon the application of force on the x axis at one end of the chain (the C-ter end) and by fixing the other end (the N-ter end), the energy of the molecule remains invariant with respect to only one degree of freedom: the rotation around the x axis. Thus, before extracting the $\langle C_{ij} \rangle$ values, we aligned each conformation of the chain with the reference structure to eliminate the contribution of this degree of freedom. The alignment was performed by adapting Kabsch's algorithm to the case of axial symmetry and no translation. Operationally, for each conformation during pulling, we applied on all the positions a matrix of rotation, Ω, given by

$$\begin{pmatrix} 1 & 0 & 0 \\ 0 & \cos\alpha & \sin\alpha \\ 0 & -\sin\alpha & \cos\alpha \end{pmatrix},$$

where α is the azimuthal angle of rotation from the reference structure. Because, to mimic the experiments, the N-ter end of the chain is kept fixed, any unfolding events at the other end of the chain leads to strong spatial correlations of the corresponding amino acids. Thus, this is not an artifact of our alignment, but an important checkpoint (see Results).

Because the unfolding of each protein is driven by force, we expect to find considerable collective motions on the direction of pulling. The full three-dimensional correlations from Eq. 2 are unlikely to provide a conclusive picture of such large collective motions before the unfolding of the corresponding region(s) in the protein structure. Therefore, to capture this behavior, we also determined the correlations between all the positions in a chain along each of the Cartesian coordinates by specializing Eq. 2 separately for the contributions of the x-, y-, and, respectively, z-direction displacements of the pairs of amino acids. Because α- and β-tub unfold according to two distinct pathways, to highlight the sets of collective motions that drive them to follow one or the other pathway, we calculated, for each peak in the FEC, the differences between the $\langle C_{ij} \rangle$ values for the major and the minor pathways.

Tension propagation

To monitor the progress of tension propagation from the point of application of force, we calculated the force on each covalent bond i, $i+1$ and we assigned it to bead i. The force is obtained from the covalent part of the potential energy function of the SOP model (Eq. 1) according to

$$f_i(t) = k\left(r_{i,i+1} - r^0_{i,i+1}\right)\left(\frac{1}{1 - \frac{\left(r_{i,i+1} - r^0_{i,i+1}\right)^2}{R_0^2}}\right). \qquad (3)$$

Similar to the approach used to determine the correlations, we computed, for each peak in the FEC, the tension on each bond as $\langle f_i \rangle$ by averaging over the same states used in the averaging of the correlations. We also monitored the degree of alignment of each covalent bond on the direction of pulling by extracting the $\langle \cos(\theta) \rangle$, where θ is the angle between the bond vector and the x axis and the average is taken as for $\langle f_i \rangle$ (23).

Evolutionary clusters determination and the clustering approach

Because the clustering approach has been detailed in previous studies (3), a qualitative discussion of the principles behind the clustering analysis, based on a variant of the statistical coupling analysis method (3) and of the clustering method (36), is given in the Supporting Material.

RESULTS

To estimate the quasiadiabaticity in our simulations, we rely on the time evolution of the native set of contacts which determine the stability of the protein conformations in our SOP model. We found a clear separation between the transitions timescales (t_{trans}) and the basin (t_{basin}) lifetimes (for example, for β-tub $\langle t_{basin} \rangle$ ~0.22 ms and $\langle t_{trans} \rangle$ ~0.03 ms) which is indicative of quasiadiabaticity.

Equilibrium pair correlations and domain motions

We calibrated the usefulness of the interresidue orientational correlations from our dynamic trajectories in revealing connections between the dynamics and the biological function of the protein, by comparing our equilibrium results with those of a previous study (37). The correlations,

calculated according to Eq. 2, and shown in Fig. S1 reveal, as detailed in the Supporting Material, the similarity between our results and this study. This ensures that our simulations reproduce the low-energy motions of the dimer.

Formation of dynamical domains during the forced-unfolding of tubulin monomers

The time evolution of the three-dimensional covariations (Eq. 2) is illustrated in Figs. 1 and 2 for α-tub and β-tub, respectively. The covariations are calculated for each near-equilibrium basin from the corresponding FEC (Fig. S2 and Fig. S3). At step 1, only the behavior of the N-ter domain distinguishes between monomers and pathways. In the major pathway for α-tub the N-ter domain is split into two subdomains, 1–65 and 66–200, which are moving anticorrelated with each other. In the minor pathway, the N-ter domain is intact. In addition, along the major pathway the 66–200 and the C-ter domains show the largest degree of internal correlations, whereas the 1–65 domain shows the least. In contrast, in the minor pathway the C-ter domain presents internal correlations that just follow the contact map. The delineation between the dynamical domains is made clear by the presence of anticorrelations between them. For example, in the major pathway, the intermediate domain is strongly anticorrelated with the C-ter domain and with the 66–200 domain. On the other hand, the C-ter domain and the 66-200 domain are strongly correlated. The C-ter domain is also moderately correlated with the 1–65 domain. In the minor pathway, due to the reduced internal correlations of the C-ter domain, this domain has fewer anticorrelations with the middle domain and with the 66–200 fragment. In β-tub, for both pathways, only the 100–200 fragment from the N-ter domain presents large internal correlations. The changes occurring at steps 2–3 (see the Supporting Material) illustrate an important difference between the monomers: only in α-tub does the integrity of the 66–200 fragment from the N-ter domain depend on the presence of an intact (folded) H12 and of the loop connecting it to H11. The unraveling of H11 at step 5, which completes the unfolding of the C-ter domain and results in perfect correlations between all its positions, induces, in the minor pathways from both monomers, the formation of positive correlations between the N-ter domain and the 216–271 (H7,H8,S7) fragment from the middle domain. Because the 216–271 region

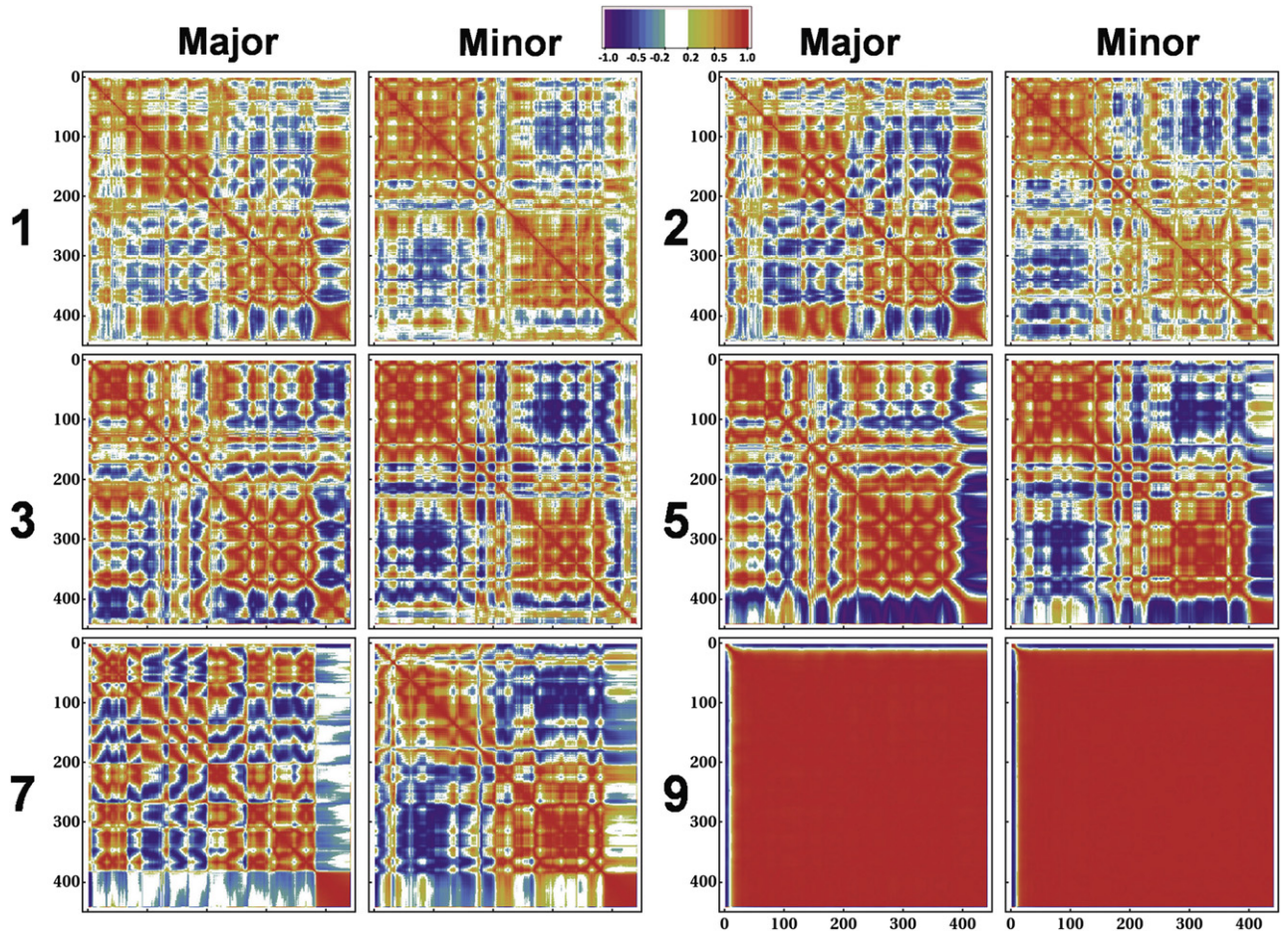

FIGURE 1 Time evolution (according to the main steps in the FEC from Fig. S2) of the pairwise correlation matrices for both unfolding pathways in α-tub. In each panel, the axes denote the residue number. Color ranges are shown on the scale bar.

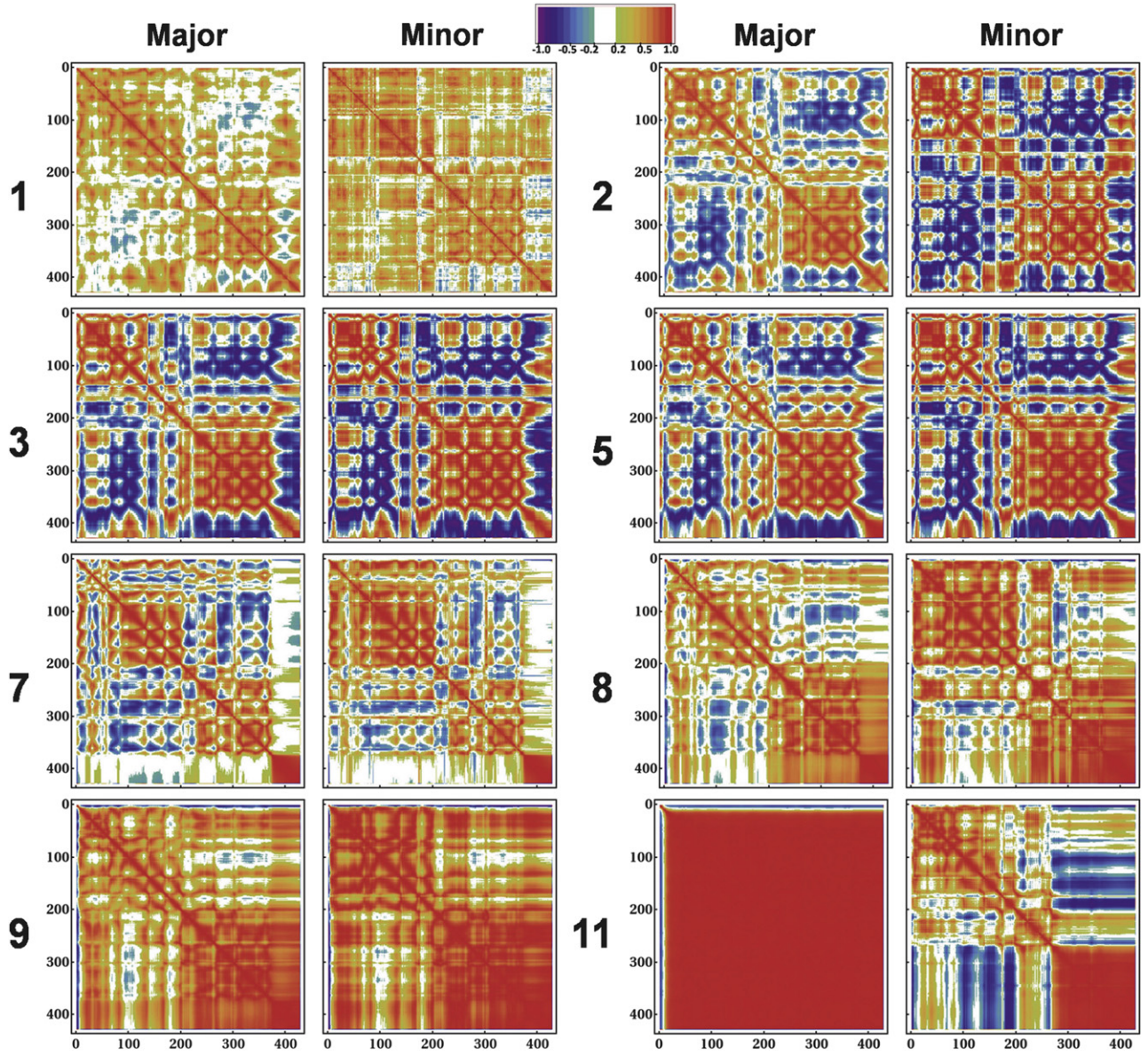

FIGURE 2 Time evolution (according to the main steps in the FEC from Fig. S3) of the correlation matrices for both unfolding pathways in β-tub.

is involved in the binding of taxol, this finding has functional implications for the dynamical instability of MTs as explained in Discussion. Details of the additional changes at step 5 and of the changes at step 7 are presented in the Supporting Material.

The major unfolding event in α-tub, occurring at step 9, is the same in both pathways: the unwinding of the N-ter domain from its 1–100 region. Thus, all positions in α-tub appear perfectly correlated in Fig. 1 (step 9). An explanation of this expected effect is provided in the Supporting Material. In contrast, for β-tub, steps 8 and 9 are intermediates of the highest peak in the FEC (Fig. S3). During these steps, in both pathways in β-tub, the folded middle domain and the unfolded C-ter domain merge to form one large domain which, in the minor pathway, is clearly anticorrelated with the almost intact N-ter domain. In the major pathway, the 1–100 region of the N-ter domain is still fragmented and it is anticorrelated with the union of the other two domains. The next unwinding event in the β-tub pathways occurs at step 11: in the major pathway, the chain unfolds from its N-term end. As expected, the correlations behave the same as during the corresponding process at step 9 in α-tub: all positions move correlated. Along the minor pathway, only the 266–427 positions move together, reflecting the unwinding of the chain from the middle domain.

Mapping the correlations on the direction of pulling

Although we determined the correlations along each of the three Cartesian directions, here we are focusing on the

covariations along the force direction. The x axis correlations for the major pathway in α-tub and for the major and minor pathways in β-tub are illustrated in Fig. S5 and, respectively, in Fig. S7 (the y- and the z-axis covariations for the two monomers are in Fig. S8, Fig. S9, Fig. S10, and Fig. S11). In α-tub these correlations indicate that, at the beginning (steps 1 and 2), only the middle domain and the 1–65 fragment of the N-ter domain present internal collective motion on the pulling direction and are also correlated between them. These correlations are therefore the reason of the split of the N-ter domain into two subdomains as found above and of the correlations between the middle domain and the first subdomain from the N-ter. Both the C-ter domain and the 66–200 fragment are absent from these two sets of correlations. This gives support to our proposal that these very distant (along the sequence) fragments of the molecule are responsible for each others' native stability against an applied force. For the major pathway of β-tub, at steps 1 and 2, each of the three domains shows some internal correlation. The N-ter and C-ter domains are also correlated between them and anticorrelated with the middle domain. This accounts for the N-ter domain being more robust to changes in β-tub than in α-tub. In addition, in β-tub the C-ter domain has internal collective motions on the x axis from the start. For the minor pathway in β-tub, only the 65–200 and the C-ter domains are correlated internally and with each other along the x axis. Steps 3 and 5 (detailed in the Supporting Material) reveal the reason behind the difference between the unfolding of the C-ter domain in the two monomers: even if in both monomers the unfolding of the C-ter domain occurs by unzipping of H12 from H11, this process is cooperative only in β-tub. The covariations in α-tub show that the C-ter positions move in the plane perpendicular to the direction of pulling before the unzipping. In contrast, in β-tub some C-ter positions move collectively on the x axis well before the unzipping starts. We also found that, for both monomers, a required event, before the beginning of unfolding in the C-ter domain, is that the middle domain positions must move collectively along the pulling direction. A common trend along all pathways and in both monomers is that, from the time the C-ter domain is unfolded and by the time the force climbs to its maximal value at step 7, the majority of correlations and anticorrelations disappear as the rest of the chain prepares to unfold (see the Supporting Material).

Tension propagation

The above findings are illustrated by the time evolution of the tension propagation (Eq. 3) inside each monomer. Fig. 3 shows that the propagation of the applied force inside the chain is delayed until step 3 because of the large initial number of noncovalent bonds. At step 3, the covalent bonds connecting the last ~10 positions in the chain all respond to tension, followed (at steps 5 and 7) by the rest of the C-ter domain (see the Supporting Material for details). Next, in both pathways from α-tub and in the major pathway for β-tub, tension is felt in the 1–100 fragment from the N-ter domain and in the unfolded C-ter domain. It is important to note that, at the beginning (in step 9 for α-tub), the tension is not uniformly distributed along the 1–100 fragment, but only on the 1–64 and the 90–100 parts because the 65–89 fragment is still folded at this time. Consequently, tension becomes uniformly distributed in this region of the chain only at step 11 upon the unfolding of S2 and H2 (65–89). A discussion of the tension propagation during the final peaks of the FEC can be found in the Supporting Material. The graphs of the cosine of the angle between the x axis and the orientation of each bond (Fig. 3), obtained following Hyeon et al. (23), indicate that, in both monomers, each unfolding event is accompanied by a jump in the $\cos(\theta)$ of all the bonds in the unfolded segment from their original value to 1. However, even if later the tension drops, the orientation along the x axis of the unfolded part remains unchanged (with $\cos(\theta)$ being constantly equal to 1), signaling the absence of any refolding.

Clustering analysis of α-tub dynamical domains and evolutionary information

To determine the sets of positions in α-tub that cluster to form dynamical domains, we performed, following the Methods and Dima and Thirumalai (3), a superparamagnetic clustering of the above correlations. We found that, at the beginning of pulling, in the major pathway there are two significant clusters, one containing a mixture of the N-ter and C-ter structural domains, and the other containing residues from the middle domain (Fig. S6 *A*). Clustering of the correlations at step 7 resulted in five clusters that depend on the pathway (as seen in Fig. S6 *B* for the major pathway and in Fig. S6 *C* for the minor pathway). Although details of the implementation and the results are given in the Supporting Material, we note that, on each pathway, the partitioning of α-tub in clusters of correlated positions is relevant for the order of unfolding along the respective pathway. The comparison between these results and the results of the bioinformatic clustering in α-tub reveals that the only evolutionarily selected cluster is the largest cluster for the major pathway.

The amplitude of the rotation around the pulling direction drives the bifurcation of the unfolding pathway in β-tub monomers

The comparison of the pair correlations, calculated from Eq. 2 using either the full three-dimensional orientations or only the corresponding x axis (pulling direction) components, reveals that the major effect leading to the unfolding of β-tub at the highest peak in the FEC is the degree of rotation, i.e., the amplitude of the angular velocity, of the yet-to-be unfolded chain fragments around the direction of pulling. For example, at the largest force peak for the unfolding of

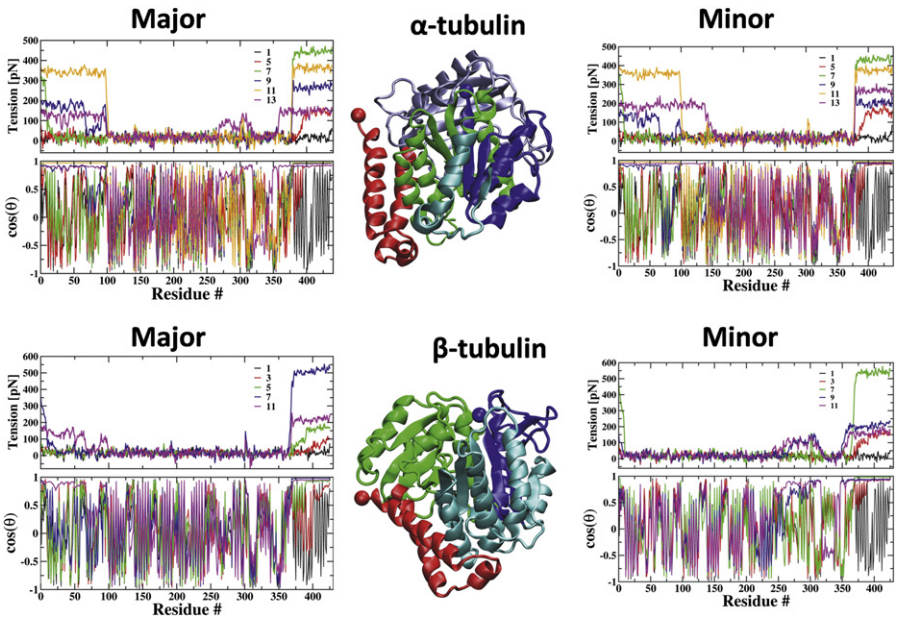

FIGURE 3 Tension propagation during the unfolding of α- and β-tub during the steps from Fig. S2 and Fig. S3. The top-left corner contains the tension and the bond orientation for the major pathway in α-tub, whereas the top-right corner is for the minor pathway in α-tub. The bottom-left and bottom-right corner show the respective entries for the major and the minor pathways in β-tub, respectively. Structural details of the related dynamical domains are in the middle plots (α-tub on top and β-tub at the *bottom*). Color scheme for structures. For α-tubulin: red, C-terminal region; light blue, middle domain (residues 215–385); green, part of the N-terminal region (residues 98–215); cyan, part of the N-terminal domain (residues 66–97); and blue, residues 1–65. The N-terminal and C-terminal residue are shown with blue and red spheres, respectively. For β-tubulin: red, C-terminal region; green, middle domain (residues 215–380); cyan, part of the N-terminal domain (residues 66–215); and blue, residues 1–65. The N-term and the C-term residues are shown as blue and red spheres, respectively.

the β-tub along the major pathway, the 1–100 (from the N-ter domain) and the 225–350 (from the middle domain) fragments behave as rigid bodies that undergo fluctuations around the azimuthal direction without large internal deformations. The time series of the azimuthal angle for each fragment (Fig. 4) reveal that, at the end of the highest peak (step 9), there is a crossover between the directions of rotation of the two fragments. More importantly, the fragment that rotates with the largest angular velocity right after the crossover is the next one to unfold. Thus, we conjecture that, at the critical force in the force-induced unfolding of β-tub, the fragment rotating with the largest angular speed is the first to unfold. The confirmation of this hypothesis is in the Supporting Material.

Formation of dynamical domains during tubulin dimer unfolding

Because the unfolding pathway in the dimer does not depend on the direction of pulling, we discuss the correlations along the pathway corresponding to the application of force to the C-ter end of β-tub with the N-ter end of α-tub kept fixed (Fig. 5). The corresponding correlations for the other two ways of pulling are in Fig. S12 (for pulling at the N-ter of α-tub) and Fig. S13 (for pulling at both the C-ter end of β-tub and at the N-ter of α-tub). Fig. 5 shows that, although the force is ramping-up (steps 1 and 2), the correlation matrices resemble the equilibration correlations: in α-tub the middle and the C-ter domains are well formed, although the N-ter domain is split into a number of fragments. In β-tub, the N-ter and the C-ter domains are strongly self-correlated, whereas the middle domain is less well structured. Due to the substantial ramping-up of the force that induces the first forced-unfolding peak (step 3), the division of the monomers into dynamical domains becomes very pronounced. In α-tub, the only distinct subdomain of its N-ter domain is 1–65, the rest being fragmented. The middle and the C-ter domains are strongly self-correlated. The 1–65 fragment is correlated with the middle domain and anticorrelated with the C-ter domain. The remainder of the N-ter domain is anticorrelated with the middle domain and correlated with the C-ter domain. This is exactly what we would have expected based on our previous finding that the dynamical stability of the 66–200 portion of the N-ter domain of α-tub depends on the stability of the C-ter domain. In β-tub, the N-ter and the C-ter domains are strongly correlated with each other, whereas the middle domain is correlated with all three domains in α-tub. In addition, the 1–65 fragment and the C-ter domain of α-tub are correlated with the entire β-tub chain. At the same time, the C-ter and N-ter domains of β-tub are anticorrelated with the middle domain of α-tub. Before the maximal force peak (step 7), the N-ter of α-tub splits into the same two parts that we encountered during the major trajectory for the monomeric α-tub: 1–65 and 66–200. However, this time the 66–200 region almost merges with the middle domain to form a large dynamical domain whose positions are loosely intercorrelated. In addition, the magnitude of the anticorrelations, present between the various dynamical regions of the two monomers, decreases. After the highest peak, which corresponds to the unraveling of the S8-S10 fragment from the middle domain of β-tub and the breaking of ~50% of the intradimer interface contacts, the still folded part of the middle domain in β-tub is no longer correlated with the middle and C-ter domains of α-tub. Still, it continues to be correlated with the N-ter domain of α-tub. After subsequent unfolding events (steps

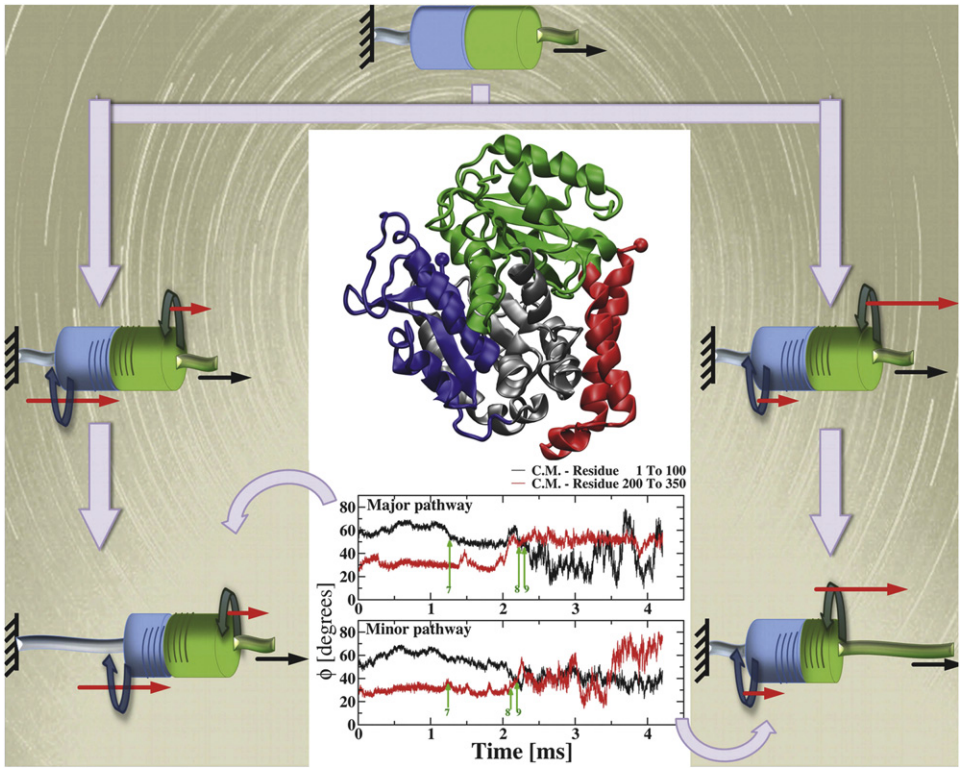

FIGURE 4 Process of pathway bifurcation in β-tub with a cartoon representation highlighting the role played by the angular velocity. The PDB structure of β-tub is in the middle and colored according to: blue, part of the N-terminal region, residues 1–100; gray, part of the N-terminal domain, residues 101–200; green, middle domain, residues 200–350; red, C-terminal domain. The cartoon depicts the two domains with the same color (*blue* and *green*). During the unfolding, these domains rotate in opposite directions (shown with *blue* and *green curved arrows*). The bifurcation in the unfolding pathway of β-tub, influenced by the angular speed (*red arrows*), is due to the unfolding of the domain rotating with the larger angular speed. The evolution of the azimuthal angle of the center of each domain is shown for the major and the minor pathways. The numbers 7–9 marked on the plots denote the beginning of the corresponding steps on the FEC shown in Fig. S3. In the major pathway, the larger flexibility and angular speed of the N-terminal domain prompts the unfolding from N-terminal region, whereas the opposite scenario is seen in the minor pathway.

9 and 11) leading to the full unfolding of the middle domain in β-tub, the correlations between the middle domain of β-tub and domains in α-tub cease to exist. The order of unfolding in the dimer is reflected also in the tension along the covalent bonds of the dimer from Fig. S14 where the only considerable force is found on the C-ter domain of β-tub and next on the middle domain of β-tub. The main dynamical domains that result from the above analysis are depicted in Fig. S14: in α-tub, the 1–65 is shown (in *light blue*) and the 66–200 is shown (in *green*); and in β-tub, the structural domains are shown (colored, respectively, in *cyan*, *orange*, and *red*).

Mapping the correlations on the direction of pulling

Based on the analysis of the x-direction component of the pairwise correlations in the dimer (Fig. S15), we concluded that, similar to our above findings in the tubulin monomers, correlated large-scale rigid body motions (rotations and translations) in the plane perpendicular to the direction of pulling give rise to the main peaks in the FEC. One such instance is the unfolding of the C-ter domain of β-tub which occurs, just as in the monomer case, by unzipping: the unfolding is driven by the collective motions of the positions in this domain in the plane perpendicular to the direction of pulling. Also, the lack of unfolding of the α-tub monomer in the dimer is due to its inability to rotate to align on the direction of pulling because it is anchored at the dimer interface (see the Supporting Material).

DISCUSSION

We showed that, based on the information from the three-dimensional correlations and from their one-dimensional projections, the unfolding process in tubulin can be followed by employing a rigid-body (RB) description of the chain (11,17,24,26,40). For both tubulin monomers and on both pathways, at the beginning of the unfolding, the only dynamical domain that overlaps well with the structural domain is the middle domain. Because the remaining two structural domains (N-ter and C-ter) appear either fragmented or intact, moving together or independent as a function of monomer and unfolding pathway, an RB-based description of the tubulin monomers cannot be more coarse-grained than: one RB for the middle domain, two RBs for the C-ter domain (one for H12 and one for H11 with the loop connecting it to H12), and five RBs for the N-ter domain (one for 1–65, one for 66–110, one for 111–140, one for 141–171, and one for 172–215). This level of description of the chain topology is appropriate only until the unfolding of the C-ter domain (up to step 5). To capture the next major unfolding event(s) from steps 7 to 11, the description of the new, near-equilibrium, chain configuration must contain different RBs (as determined from the smallest regions that

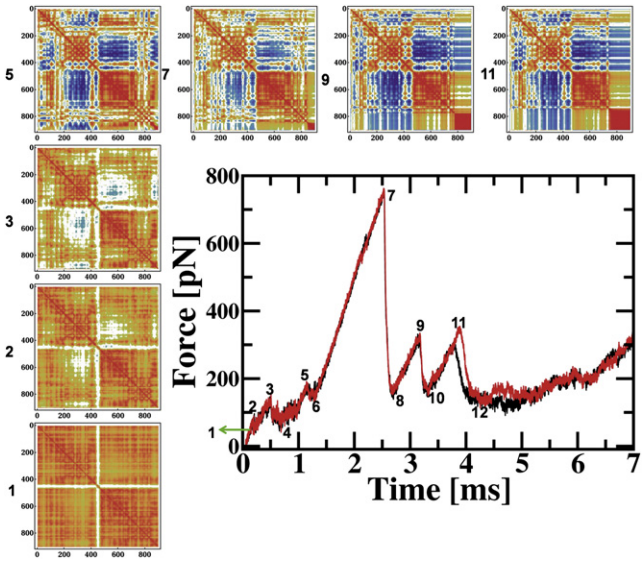

FIGURE 5 Correlations during the unfolding of dimer when the N-ter of α-tub is fixed and the C-ter of β-tub is pulled. In the center, the FEC is shown with the steps for which the correlations were computed (labeled 1–12). Along the FEC the individual correlations are shown in clockwise arrangement. The color-scale of the correlation is the same as in the Fig. 1.

show strong autocorrelations along at least one pathway in a monomer): one RB for the C-ter domain, four RBs for the middle domain (one for 216–239, one for 240–273, one for 274–350, and one for 351–380), and seven RBs for the N-ter domain (one for 1–65, one for 66–80, one for 80–96, one for 97–110, one for 111–127, one for 128–140, and one for 141–215). A different RB-based description of the chain topology can be employed to describe the unfolding of the tubulin dimer up to the unfolding of the C-ter domain in β-tub: α-tub is one RB, whereas β-tub is three RBs (one for the N-ter and middle domains, one for H12, and one for H11 and the loop connecting it to H12). However, following the unraveling of the C-ter domain, each monomer must be described at the level introduced above for steps 7–11. Thus, our finding that the application of net constraints on a molecule induces the formation of dynamical domains, which do not overlap perfectly with the structural domains, agrees with previous studies (6,41). However, unlike previous reports, our study highlights that these domains evolve with time and they depend crucially on the extent of the confinement of the chain as in the dimer case.

Along the minor pathways of both monomers, we found that the unfolding of H11 induces the formation of positive correlations between the N-ter domain and the 216–271 (H7,H8,S7) fragment from the middle domain. This has important consequences for the proper functioning of the dimer. The 216–271 fragment is part of the taxol binding site in β-tub and a recent MD study of the effect of taxol binding on the flexibility of tubulin (42) found that, upon taxol binding to β-tub, this region shows signs of partial melting of H7. They also found increased dynamics in the H1-S2 loop which is close to the taxol binding site, but more importantly in the T1-T5 loops and in H11, which are distant from that site. Therefore, our finding that a large change in H11 triggers correlated changes in the other regions identified by Mitra and Sept (42) indicates that the binding of taxol to tubulin does not occur through an induced fit mechanism, but rather by a shift in the population of tubulin conformers (43). As the correlation between the above chain fragments occurs only along the minor pathway from each monomer, the population of this state is small in the absence of taxol. Because the binding of taxol shifts the population of the state to large values and it is known that taxol blocks the depolymerization of MTs, the reason that the collective motions among T1-T5, the H1-S2 loop, H7-S7, and H11 are found only along the minor pathways is because they can lead to the blocking of the dynamic instability of MTs with grave functional consequences.

Finding that the order of unfolding of fragments in large, multidomain proteins such as β-tub depends on the amplitude of the angular velocity of domains along the direction of pulling offers a new microscopic insight into the anisotropic deformation response. This behavior was found by earlier studies that investigated the influence of the pulling direction on the magnitude of the unfolding force and, more importantly, on the identity of the unfolding pathway as done, for example, in the green fluorescent protein by Dietz et al. (44). Moreover, this result lends support to the experimental finding that, to increase the likelihood of unraveling of complex cytoskeletal structures under moderate force values, molecular motors use a combination of pulling and torsion rather than just simple pulling (45).

Our study shows that, in general, to monitor the propagation of tension along the molecule and its relationship with the kinetics of unfolding in the chain, one needs to monitor both the tension propagation along the covalent bonds of the chain and their degree of orientation along the axis of pulling (as seen in Fig. 3). Using only the information from tension propagation can obscure possible refolding events. Conversely, using only the orientation information fails to reveal the temporary decrease in tension along the unfolded segments, whereas the still folded portions of the chain start to experience tension buildup.

SUPPORTING MATERIAL

Additional text, 15 figures, and references are available at http://www.biophysj.org/biophysj/supplemental/S0006-3495(09)01685-3.

R.I.D. is grateful to Prof. D. Thirumalai and to Prof. V. Barsegov for useful discussions.

This project has been supported in part by a University of Cincinnati URC Postdoctoral Research Fellowship (to H.J.) and by the National Science Foundation grant No. MCB-0845002 (to R.I.D.).

REFERENCES

1. Kern, D., and E. R. Zuiderweg. 2003. The role of dynamics in allosteric regulation. *Curr. Opin. Struct. Biol.* 13:748–757.
2. Hyeon, C., G. H. Lorimer, and D. Thirumalai. 2006. Dynamics of allosteric transitions in GroEL. *Proc. Natl. Acad. Sci. USA.* 103: 18939–18944.
3. Dima, R. I., and D. Thirumalai. 2006. Determination of network of residues that regulate allostery in protein families using sequence analysis. *Protein Sci.* 15:258–268.
4. Chen, J., R. I. Dima, and D. Thirumalai. 2007. Allosteric communication in dihydrofolate reductase: signaling network and pathways for closed to occluded transition and back. *J. Mol. Biol.* 374:250–266.
5. Perez-Jimenez, R., A. P. Wiita, …, J. M. Fernandez. 2008. Force-clamp spectroscopy detects residue co-evolution in enzyme catalysis. *J. Biol. Chem.* 283:27121–27129.
6. Potestio, R., F. Pontiggia, and C. Micheletti. 2009. Coarse-grained description of protein internal dynamics: an optimal strategy for decomposing proteins in rigid subunits. *Biophys. J.* 96:4993–5002.
7. Howard, J., and A. A. Hyman. 2003. Dynamics and mechanics of the microtubule plus end. *Nature.* 422:753–758.
8. Kis, A., S. Kasas, …, L. Forro. 2002. Nanomechanics of microtubules. *Phys. Rev. Lett.* 89:248101.
9. de Pablo, P., I. Schaap, …, C. Schmidt. 2003. Deformation and collapse of microtubules on the nanometer scale. *Phys. Rev. Lett.* 91:098101.
10. Zink, M., and H. Grubmüller. 2009. Mechanical properties of the icosahedral shell of Southern Bean Mosaic virus: a molecular dynamics study. *Biophys. J.* 96:1350–1363.
11. Kim, M. K., R. L. Jernigan, and G. S. Chirikjian. 2005. Rigid-cluster models of conformational transitions in macromolecular machines and assemblies. *Biophys. J.* 89:43–55.
12. Nogales, E., M. Whittaker, …, K. H. Downing. 1999. High-resolution model of the microtubule. *Cell.* 96:79–88.
13. Nogales, E., and H. W. Wang. 2006. Structural intermediates in microtubule assembly and disassembly: how and why? *Curr. Opin. Cell Biol.* 18:179–184.
14. Schek, 3rd, H. T., M. K. Gardner, …, A. J. Hunt. 2007. Microtubule assembly dynamics at the nanoscale. *Curr. Biol.* 17:1445–1455.
15. Nogales, E., S. G. Wolf, and K. H. Downing. 1998. Structure of the α/β tubulin dimer by electron crystallography. *Nature.* 391:199–203.
16. Kasas, S., A. Kis, …, S. Catsicas. 2004. Mechanical properties of microtubules explored using the finite elements method. *ChemPhysChem.* 5:252–257.
17. Molodtsov, M. I., E. A. Ermakova, …, F. I. Ataullakhanov. 2005. A molecular-mechanical model of the microtubule. *Biophys. J.* 88: 3167–3179.
18. VanBuren, V., L. Cassimeris, and D. J. Odde. 2005. Mechanochemical model of microtubule structure and self-assembly kinetics. *Biophys. J.* 89:2911–2926.
19. Zeiger, A. S., and B. E. Layton. 2008. Molecular modeling of the axial and circumferential elastic moduli of tubulin. *Biophys. J.* 95:3606–3618.
20. Dent, E. W., and K. Kalil. 2001. Axon branching requires interactions between dynamic microtubules and actin filaments. *J. Neurosci.* 21:9757–9769.
21. Roll-Mecak, A., and R. D. Vale. 2008. Structural basis of microtubule severing by the hereditary spastic paraplegia protein spastin. *Nature.* 451:363–367.
22. Dima, R. I., and H. Joshi. 2008. Probing the origin of tubulin rigidity with molecular simulations. *Proc. Natl. Acad. Sci. USA.* 105:15743–15748.
23. Hyeon, C., R. I. Dima, and D. Thirumalai. 2006. Pathways and kinetic barriers in mechanical unfolding and refolding of RNA and proteins. *Structure.* 14:1633–1645.
24. Tama, F., F. X. Gadea, …, Y. H. Sanejouand. 2000. Building-block approach for determining low-frequency normal modes of macromolecules. *Proteins.* 41:1–7.
25. Zheng, W. J., B. R. Brooks, …, D. Thirumalai. 2005. Network of dynamically important residues in the open/closed transition in polymerases is strongly conserved. *Structure.* 13:565–577.
26. Yesylevskyy, S. O., V. N. Kharkyanen, and A. P. Demchenko. 2006. Hierarchical clustering of the correlation patterns: new method of domain identification in proteins. *Biophys. Chem.* 119:84–93.
27. Keskin, O., S. R. Durell, …, D. G. Covell. 2002. Relating molecular flexibility to function: a case study of tubulin. *Biophys. J.* 83:663–680.
28. Medina-Noyola, M., and J. Keizer. 1981. Spatial correlations in nonequilibrium systems: the effect of diffusion. *Physica.* 107:437–463.
29. Noolandi, J., and K. M. Hong. 1984. Non-equilibrium correlation function of a reptating chain. *J. Phys. Lett.* 45:L149–L157.
30. Zwanzig, R. 2001. Nonequilibrium Statistical Mechanics. Oxford University Press, Oxford, UK.
31. Evans, E. 1998. Energy landscapes of biomolecular adhesion and receptor anchoring at interfaces explored with dynamic force spectroscopy. *Faraday Discuss.* 111:1–16.
32. Hummer, G., and A. Szabo. 2003. Kinetics from nonequilibrium single-molecule pulling experiments. *Biophys. J.* 85:5–15.
33. Hyeon, C., and D. Thirumalai. 2007. Measuring the energy landscape roughness and the transition state location of biomolecules using single molecule mechanical unfolding experiments. *J. Phys. Condens. Matter.* 19:113101–113127.
34. Dudko, O. K., G. Hummer, and A. Szabo. 2008. Theory, analysis, and interpretation of single-molecule force spectroscopy experiments. *Proc. Natl. Acad. Sci. USA.* 105:15755–15760.
35. Wolynes, P. G., J. N. Onuchic, and D. Thirumalai. 1995. Navigating the folding routes. *Science.* 167:1619–1620.
36. Blatt, M., S. Wiseman, and E. Domany. 1996. Superparamagnetic clustering of data. *Phys. Rev. Lett.* 76:3251–3254.
37. Berman, H. M., J. Westbrook, …, P. E. Bourne. 2000. The Protein Data Bank. *Nucleic Acids Res.* 28:235–242.
38. Rief, M., M. Gautel, …, H. E. Gaub. 1997. Reversible unfolding of individual titin immunoglobulin domains by AFM. *Science.* 276: 1109–1112.
39. Kabsch, W. 1976. A solution for the best rotation to relate two sets of vectors. *Acta. Crystal.* 32:922–923.
40. Essiz, S., and R. D. Coalson. 2006. A rigid-body Newtonian propagation scheme based on instantaneous decomposition into rotation and translation blocks. *J. Chem. Phys.* 124:144116–144126.
41. Knaggs, M. H., F. R. Salsbury, …, J. S. Fetrow. 2009. Insights into correlated motions and long-range interactions in CheY derived from molecular dynamics simulations. *Biophys. J.* 92:2062–2079.
42. Mitra, A., and D. Sept. 2008. Taxol allosterically alters the dynamics of the tubulin dimer and increases the flexibility of microtubules. *Biophys. J.* 95:3252–3258.
43. Kumar, S., B. Ma, …, R. Nussinov. 2000. Folding and binding cascades: dynamic landscapes and population shifts. *Protein Sci.* 9:10–19.
44. Dietz, H., F. Berkemeier, …, M. Rief. 2006. Anisotropic deformation response of single protein molecules. *Proc. Natl. Acad. Sci. USA.* 103:12724–12728.
45. Tsuda, Y., H. Yasutake, …, T. Yanagida. 1996. Torsional rigidity of single actin filaments and actin-actin bond breaking force under torsion measured directly by in vitro micromanipulation. *Proc. Natl. Acad. Sci. USA.* 93:12937–12942.